

Orbital-free effective embedding potential at nuclear cusp

Juan Maria Garcia Lastra^a, Jakub W. Kaminski,
and Tomasz A. Wesolowski

Université de Genève,
Département de Chimie Physique
30, quai Ernest-Ansermet,
CH-1211 Genève 4, Switzerland

^a Universidad del País Vasco
Departamento de Física de Materiales
E-20018 Donostia-San Sebastian, Spain

October 31, 2018

Abstract

A new approach to approximate the kinetic-energy-functional dependent component ($v_t[\rho_A, \rho_B](\vec{r})$) of the effective potential in one-electron equations for orbitals embedded in a frozen density environment (Eqs. 20-21 in [Wesolowski and Warshel, *J. Phys. Chem.* **97**, (1993) 8050]) is proposed. The exact limit for v_t at $\rho_A \rightarrow 0$ and $\int \rho_B d\vec{r} = 2$ is enforced. The significance of this limit is analysed formally and numerically for model systems including a numerically solvable model and real cases where $\int \rho_B d\vec{r} = 2$. A simple approximation to $v_t[\rho_A, \rho_B](\vec{r})$ is constructed which enforces the considered limit near nuclei in the environment. Numerical examples are provided to illustrate the numerical significance of the considered limit for real systems - intermolecular complexes comprising, non-polar, polar, charged constituents. Imposing the limit improves significantly the quality of the approximation to $v_t[\rho_A, \rho_B](\vec{r})$ for systems comprising charged components. For complexes comprising neutral molecules or atoms the improvement occurs as well but it is numerically insignificant.

1 Introduction

Numerical methods to study electronic structure in condensed matter use mainly techniques developed for periodic systems. In many cases, however, methods developed for finite systems are also used. They are especially adequate for ionic solids, liquids, molecular crystals, clusters of molecules, for instance, to study features of the electronic structure which are local in character. In such a case, the electronic structure is modelled only in some well-defined region in space of direct relevance. The effect of the atoms outside of this selected region (referred to as environment in this work) is taken into account by some *embedding potential*. Different strategies are applied in practice to represent the embedding potential. They differ in the choice of descriptor of the environment. The roughest approximation is to neglect the environment entirely. Such simplification is commonly used to study chemical bonding and reactivity in condensed phase if the solvent in which the reaction takes place is known to play a secondary role. Representing the environment (discrete or continuous, polarisable or not) by the electric field it generates, makes it possible to take into account the effect of the environment [1, 2]. Such classical treatment of the effect of the environment on the electronic structure is commonly used both in chemistry and in materials science (for review see Ref. [3]). The embedding potential in such methods is obviously orbital-free. It is, however, not exact because the quantum statistics nature of electrons is completely neglected. Taking into account the fermion nature of electrons might proceed by following a similar strategy as the one applied by Phillips and Kleinman in the construction of pseudopotentials in order to eliminate explicit treatment of core electrons [4]. For recent developments along these lines, see Ref. [5].

Using the following elements of the Hohenberg-Kohn-Sham formulation of density functional theory: Hohenberg-Kohn theorems [6], a reference system of non-interacting electrons [7], and the corresponding density functional of the kinetic energy ($T_s[\rho]$) [8] in particular, leads to the embedding potential which is *exact* in the limit of exact functionals and *orbital-free* i.e. does not involve other descriptors of the environment than its electron density [9]. The pure-state non-interacting v -representable electron density ρ_A^{min} , such that added to some arbitrarily chosen density associated with the environment (ρ_B) minimises the Hohenberg-Kohn energy functional for the whole system, can be obtained from the following one-electron equations (Eqs. 20-21 in

Ref. [9]):

$$\left[-\frac{1}{2}\nabla^2 + v_{eff}^{KSCED}[\rho_A, \rho_B; \vec{r}]\right] \phi_i^A = \epsilon_i^A \phi_i^A \quad i = 1, N^A \quad (1)$$

where $\rho_A = 2 \sum_i^{N^A} |\phi_i|^2$ and $v_{eff}^{KSCED}[\rho_A, \rho_B; \vec{r}]$ denotes a local potential which depends only on electron densities ρ_A and ρ_B . The label KSCED (Kohn-Sham Equations with Constrained Electron Density) is used here to indicate that the local potential differs from that in Kohn-Sham equations [7] for either the total system ($v^{KS}[\rho_A + \rho_B; \vec{r}]$) or the isolated subsystem A ($v^{KS}[\rho_A; \vec{r}]$). Also the one-electron functions ($\{\phi_i^A\}$) obtained from Eq. 1 are not optimal orbitals in neither Kohn-Sham systems. Atomic units are applied in all formulas which are given for spin unpolarised systems.

The total effective potential in Eq. 1 is the sum of the conventional Kohn-Sham effective potential $v_{eff}^{KS}[\rho_A + \rho_B; \vec{r}]$ for the whole system evaluated for the electron density $\rho = \rho_A + \rho_B$ and another local potential ($v_t[\rho_A, \rho_B](\vec{r})$):

$$v_{eff}^{KSCED}[\rho_A, \rho_B; \vec{r}] = v_{eff}^{KS}[\rho_A + \rho_B; \vec{r}] + v_t[\rho_A, \rho_B](\vec{r}) \quad (2)$$

where $v_t[\rho_A, \rho_B](\vec{r})$ involves functional derivatives of the functional $T_s[\rho]$:

$$v_t(\vec{r}) = v_t[\rho_A, \rho_B](\vec{r}) = \left. \frac{\delta T_s[\rho]}{\delta \rho} \right|_{\rho=\rho_A+\rho_B} - \left. \frac{\delta T_s[\rho]}{\delta \rho} \right|_{\rho=\rho_A} \quad (3)$$

Note that no restriction is made concerning the overlap between ρ_A and ρ_B in real space. The potential $v_t[\rho_A, \rho_B](\vec{r})$ can be alternatively expressed as:

$$v_t[\rho_A, \rho_B](\vec{r}) = \left. \frac{\delta T_s^{nad}[\rho, \rho_B]}{\delta \rho} \right|_{\rho=\rho_A} \quad (4)$$

where $T_s^{nad}[\rho_A, \rho_B]$ denotes the following difference:

$$T_s^{nad}[\rho_A, \rho_B] = T_s[\rho_A + \rho_B] - T_s[\rho_A] - T_s[\rho_B] \quad (5)$$

For the sake of the subsequent discussions, it is convenient to split the total effective potential $v_{eff}^{KSCED}[\rho_A, \rho_B; \vec{r}]$ into two components: the Kohn-Sham effective potential for the isolated subsystem A ($v_{eff}^{KS}[\rho_A; \vec{r}]$), which is

ρ_B independent, and the remaining part representing the environment:

$$v_{eff}^{KSCED}[\rho_A, \rho_B; \vec{r}] = v_{eff}^{KS}[\rho_A; \vec{r}] + v_{emb}^{KSCED}[\rho_A, \rho_B; \vec{r}] \quad (6)$$

where

$$\begin{aligned} v_{emb}^{KSCED}[\rho_A, \rho_B; \vec{r}] &= v_{ext}^B(\vec{r}) + \int \frac{\rho_B(\vec{r}')}{|\vec{r}' - \vec{r}|} d\vec{r}' \\ &+ \left. \frac{\delta E_{xc}[\rho]}{\delta \rho} \right|_{\rho=\rho_A+\rho_B} - \left. \frac{\delta E_{xc}[\rho]}{\delta \rho} \right|_{\rho=\rho_A} + v_t[\rho_A, \rho_B](\vec{r}) \end{aligned} \quad (7)$$

where $E_{xc}[\rho]$ denotes the Kohn-Sham functional of the exchange-correlation energy [7].

Orbital-free effective embedding potential given in Eq. 7, and its $v_t[\rho_A, \rho_B](\vec{r})$ component in particular, are used in various types of multi-level numerical simulations (for a review, see Ref. [10] or Refs. [11, 12, 13, 14, 15, 16, 17, 18, 19, 20] for representative recent reports). Such simulations deal with condensed matter systems, for which the electronic features of a selected subsystem (subsystem A) are subject to detailed investigation whereas ρ_B is subject to additional simplifications. Other formal frameworks use also $v_t[\rho_A, \rho_B](\vec{r})$ such as: Cortona's formulation of density functional theory [21], where ρ_B is not an assumed quantity but a result of fully variational calculations [21, 22, 24, 23, 25] or linear-response time-dependent density-functional-theory description of electronic excitations localised in embedded systems [26, 27]. Finally, the orbital-free effective embedding potential given in Eq. 7, and its $v_t[\rho_A, \rho_B](\vec{r})$ component in particular, are used in combination with traditional wave-function based methods by Carter and collaborators (see for instance Ref. [28]). For the formal analysis of applicability of such a combination, see Ref. [29] which shows that the exact embedding potential in such a case always comprises the $v_t[\rho_A, \rho_B](\vec{r})$ component.

In practical applications, $v_t[\rho_A, \rho_B](\vec{r})$ is not used but some analytic expressions approximating this quantity ($\tilde{v}_t[\rho_A, \rho_B](\vec{r})$) for the obvious sake of practical advantages. This replacement results in errors in all derived quantities which will be referred to as *\tilde{v}_t -induced errors*. In each case, $\tilde{v}_t[\rho_A, \rho_B](\vec{r})$ is obtained by using analytic form of an approximated functional $\tilde{T}_s[\rho]$ into

Eqs. 3-5. We will refer to such $\tilde{v}_t[\rho_A, \rho_B](\vec{r})$ as *decomposable* because the analytic form of all relevant quantities: $\tilde{T}_s[\rho]$, $\tilde{T}_s^{nad}[\rho_A, \rho_B]$, and $\tilde{v}_t[\rho_A, \rho_B](\vec{r})$, is available. If the form of the used $\tilde{T}_s[\rho]$ comprises only low-level gradient-expansion [30] contributions, the corresponding decomposable $\tilde{v}_t[\rho_A, \rho_B](\vec{r})$ violates the exact limit for $v_t[\rho_A, \rho_B](\vec{r})$ at $\rho_A \rightarrow 0$ and $\int \rho_B d\vec{r} = 2$ (see Appendix A). Our interest in the local behaviour of $v_t[\rho_A, \rho_B](\vec{r})$ at this limit is motivated by the fact that the corresponding conditions occur if ρ_B comprises two electrons tightly bound to a distant nucleus in the environment such as in the case of the helium atom, Li^+ cation, Be^{2+} , etc. We expect that they are relevant also for heavier nuclei if in a volume element centred on the nucleus ρ_B is dominated by a doubly-occupied orbital.

The present work focuses on the investigation whether the considered exact limit is of any practical relevance. To this end, we apply the following strategy: *i*) We use a model system (Appendix B), for which the conditions $\rho_A \rightarrow 0$ and $\int \rho_B d\vec{r} = 2$ apply rigorously, to analyse the importance of enforcing the correct local behaviour of $\tilde{v}_t[\rho_A, \rho_B](\vec{r})$. *ii*) We construct a simple approximation to $v_t[\rho_A, \rho_B](\vec{r})$ obeying the considered exact limit in the vicinity of nuclei and analyse the numerical significance of imposing the considered condition in real systems where the conditions $\rho_A \rightarrow 0$ and $\int \rho_B d\vec{r} = 2$ do not apply rigorously.

Our ultimate goal is a new approximation to $v_t[\rho_A, \rho_B](\vec{r})$ which can be inexpensively evaluated in practice and obeys as much as possible of the relevant exact properties. It should be pointed out in this context that the position-dependency of $v_t[\rho_A, \rho_B](\vec{r})$ is the result of non-homogeneity of ρ_A and/or ρ_B . Therefore, the symbol $v_t[\rho_A, \rho_B](\vec{r})$ (or $\tilde{v}_t[\rho_A, \rho_B](\vec{r})$ if approximated) is used throughout this work to indicate that this local quantity is a functional of ρ_A and ρ_B . Explicit position dependence is strongly undesired in density-functional-theory based methods because it is not straightforward to obtain *i*) such potential as a functional derivative of some density functional, and *ii*) functional derivatives of such potential needed in some formal frameworks [26, 27]. General symbols such v_t or $v_t(\vec{r})$ are used in some discussions where the issue of explicit position-dependence is not relevant.

2 Conventional (decomposable) strategies to approximate $v_t[\rho_A, \rho_B](\vec{r})$

Before proceeding to the construction of the desired approximation to $v_t[\rho_A, \rho_B](\vec{r})$ obeying the considered limit, we overview the conventional construction of approximation to $v_t[\rho_A, \rho_B](\vec{r})$ and the local behaviour near a nucleus of the obtained potential. The conventional strategy, which is applied in our own works and the works by others so far, is to start from some explicit density functional $\tilde{T}_s[\rho]$ and to use its analytic form to derive the corresponding approximate expression for $T_s^{nad}[\rho_A, \rho_B]$:

$$T_s^{nad}[\rho_A, \rho_B] \approx \tilde{T}_s^{nad}[\rho_A, \rho_B] = \tilde{T}_s[\rho_A + \rho_B] - \tilde{T}_s[\rho_A] - \tilde{T}_s[\rho_B] \quad (8)$$

and to use the obtained analytic expression to obtain $\tilde{v}_t[\rho_A, \rho_B](\vec{r})$ by means of functional differentiation.

$$v_t[\rho_A, \rho_B](\vec{r}) \approx \tilde{v}_t[\rho_A, \rho_B](\vec{r}) = \left. \frac{\delta \tilde{T}_s^{nad}[\rho, \rho_B]}{\delta \rho} \right|_{\rho=\rho_A} \quad (9)$$

This strategy can be applied for any approximated functional $\tilde{T}_s[\rho]$ provided its form makes it possible to obtain the analytic expression for $\tilde{v}_t[\rho_A, \rho_B](\vec{r})$. Simple functionals $\tilde{T}_s[\rho]$, which depend explicitly on densities and their gradients, are of particular practical interest. They lead to $\tilde{v}_t[\rho_A, \rho_B](\vec{r})$ which depends explicitly only on ρ_A and ρ_B and their first- and second derivatives. In the original work by Cortona [21], where the subsystem formulation of density functional theory was introduced, a decomposable $\tilde{v}_t[\rho_A, \rho_B](\vec{r})$ derived from the Thomas-Fermi [31] kinetic energy functional was used to study ionic solids. In our own works, only decomposable $\tilde{v}_t[\rho_A, \rho_B](\vec{r})$ derived from gradient-dependent approximations to $T_s[\rho]$ were considered so far (see for instance the analyses of their accuracy in Ref. [32, 33] or their recent applications in multi-level computer simulations of condensed matter [16]).

Thomas-Fermi kinetic energy functional [31], which is exact for the uniform electron gas, leads to the following approximate expression for $T_s^{nad}[\rho_A, \rho_B]$:

$$\tilde{T}_s^{nad(TF)}[\rho_A, \rho_B] = C_{TF} \int \left((\rho_A + \rho_B)^{5/3} - \rho_A^{5/3} - \rho_B^{5/3} \right) d\vec{r} \quad (10)$$

where $C_{TF} = \frac{3}{10}(3\pi^2)^{2/3}$.

The associated expression for $\tilde{v}_t^{TF}[\rho_A, \rho_B](\vec{r})$ reads:

$$\tilde{v}_t^{TF}[\rho_A, \rho_B](\vec{r}) = \frac{5}{3} C_{TF} \left((\rho_A + \rho_B)^{2/3} - \rho_A^{2/3} \right) \quad (11)$$

Approximating $T_s[\rho]$ by means of the gradient expansion of the kinetic energy [30] truncated to the second order leads to the following approximate expression for $T_s^{nad}[\rho_A, \rho_B]$ [9]:

$$\tilde{T}_s^{nad(GEA2)}[\rho_A, \rho_B] = T_s^{nad(TF)}[\rho_A, \rho_B] - \frac{1}{72} \int \frac{|\rho_A \nabla \rho_B - \rho_B \nabla \rho_A|^2}{\rho_A \rho_B (\rho_A + \rho_B)} d\vec{r} \quad (12)$$

The associated expression for $\tilde{v}_t^{GEA2}[\rho_A, \rho_B](\vec{r})$ is given in Ref. [9].

For the the group of gradient-dependent approximations to $T_s[\rho]$ of the *generalised gradient approximation* form [32, 34] the analytic expression for $\tilde{T}_s^{nad}[\rho_A, \rho_B]$ reads:

$$\tilde{T}_s^{nad(GGA)}[\rho_A, \rho_B] = C_{TF} \int \left[(\rho_A + \rho_B)^{5/3} F(s_{AB}) - \rho_A^{5/3} F(s_A) - \rho_B^{5/3} F(s_B) \right] d\vec{r} \quad (13)$$

where $F^{GGA}(s)$ (*enhancement factor*) depends on a dimensionless quantity $s = \frac{|\nabla \rho|}{2(3\pi^2)^{1/3} \rho^{4/3}}$ (*reduced density gradient*). Various analytic forms of $F^{GGA}(s)$ were proposed in the literature [35, 36, 37, 38]. The associated analytic expression for $\tilde{v}_t^{GGA}[\rho_A, \rho_B](\vec{r})$ is given in Ref. [23]. It is worthwhile to notice that the GGA form is flexible and includes $\tilde{T}^{TF}[\rho]$ and $\tilde{T}^{GEA2}[\rho]$ as special cases. Numerical values of s provide useful information about shell structure and the distance from the nucleus in atoms [39]. For an atom, s is known to be small near the nucleus, reach the values of about 3 in the valence region, and diverge exponentially to $+\infty$ at large distances. In molecules, it behaves similarly with a noticeable exception of stationary points of electron density (bond midpoints for instance) where $s = 0$. Each approximated functional given in Eqs. 10-13 comprises a dominant Thomas-Fermi component and satisfies two exact conditions:

- $T_s[\rho_A + \rho_B] - T_s[\rho_A] - T_s[\rho_B] = 0$ for non-overlapping ρ_A and ρ_B .
- For uniform ρ_A and ρ_B , they recover the exact analytical expression for $T_s[\rho_A + \rho_B] - T_s[\rho_A] - T_s[\rho_B]$.

The common feature of each among the above approximations for $T_s[\rho]$ is that none of them yields the exact analytic form of $v_t[\rho_A, \rho_B](\vec{r})$ at $\rho_A \rightarrow 0$ and $\int \rho_B d\vec{r} = 2$ (see Appendix A):

$$v_t[\rho_A, \rho_B](\vec{r}) \rightarrow v_t^{limit}[\rho_B](\vec{r}) = \frac{1}{8} \frac{|\nabla \rho_B|^2}{\rho_B^2} - \frac{1}{4} \frac{\nabla^2 \rho_B}{\rho_B} \quad (14)$$

The expression given in Eq. 11, which provides the dominant contribution to gradient-expansion based approximations to $v_t[\rho_A, \rho_B](\vec{r})$ does not comprise the relevant term at all whereas the second-order term provides only 1/9 of the exact expression. Figure 1 shows $\tilde{v}_{emb}^{KSCEd(LDA)}[\rho_A, \rho_B](\vec{r})$ for a spherically symmetric case: $\rho_B = \rho_{He}$, $v_{ext}^B(\vec{r}) = -2/r$, and $\rho_A \rightarrow 0$, which represents a helium atom far from subsystem A . In the Figure as well as in the following discussion, r denotes the distance from the considered nucleus. The potential in the figure shows the features which are common also for heavier atoms if gradient expansion based approximations to $T_s[\rho]$ are used to derive $v_t[\rho_A, \rho_B](\vec{r})$: a very narrow and deep well (reaching $-\infty$) centred on the nucleus and surrounding it repulsive shell. The $v_t[\rho_A, \rho_B](\vec{r})$ component of the shown embedding potential is finite at the nucleus instead of behaving as $\frac{\zeta}{r}$. Note that the exact term has the same form as the potential due to Coulomb attraction by the nucleus of the charge Z . Therefore, the exact v_t partially compensates this attraction to some extent because ζ is smaller than Z [40]. For the particular case considered in the Figure, the missing $\frac{\zeta}{r}$ component does not lead to any bound states (Appendix B). In general, however, the wrong asymptotic of the singularity at the nucleus, can lead to an unphysical transfer of electron density from the investigated system to its environment (charge-leak [41]). This can occur if the artificially attractive (not sufficiently repulsive) approximation to the orbital-free effective embedding potential generates a bound state in the environment of the energy which is lower than the eigenvalue of the highest occupied embedded orbital associated with embedded subsystem A . Numerical cases confirming such scenario are known [42, 43]. Moreover, the numerical solution of the Schrödinger equation with $\tilde{v}_{emb}^{KSCEd(LDA)}[\rho_A, \rho_B](\vec{r})$ for $\rho_B = \rho_{Li^+}$ and the external potential of the $-\frac{3}{r}$ form, shows a deeply lying node-less bound state of the energy -0.209665 hartree with the maximum of the radial electron density at $r^{max} = 2.912$ bohr (Appendix B). The above observations indicate that decomposable $\tilde{v}_t[\rho_A, \rho_B](\vec{r})$ obtained from low-order gradient-expansion based approximations to $T_s[\rho]$ might not be adequate for, at least, Li^+ cations in the environment. The fact that the bound state associated with an atom in the environment is too tightly bound to the nucleus indicate, however, that the problem might be also present in atoms comprising more electrons.

In a subsequent section, a simple approximation to $v_t[\rho_A, \rho_B](\vec{r})$ is constructed based on these observations. In principle, the exact limit should be applied in any volume element in which ρ_A vanishes and ρ_B is obtained

from a doubly occupied orbital. In the proposed construction, the exact limit is imposed only at volume elements near heavier-than-hydrogen nuclei expecting that the considered condition is most relevant there.

3 Building-in the exact limit for $v_t[\rho_A, \rho_B](\vec{r})$ at $\rho_A \longrightarrow 0$ and $\int \rho_B d\vec{r} = 2$.

The aforementioned flaws of decomposable strategy to construct gradient- and Laplacian dependent approximations to $v_t[\rho_A, \rho_B](\vec{r})$ suggest a bottom-up approach in which $v_t[\rho_A, \rho_B](\vec{r})$ is directly a target. A given approximated potential $\tilde{v}_t[\rho_A, \rho_B](\vec{r})$ will be referred to as *non-decomposable* if the analytic form of its two individual components $\left. \frac{\delta \tilde{T}_s[\rho]}{\delta \rho} \right|_{\rho=\rho_A+\rho_B}$ and $\left. \frac{\delta \tilde{T}_s[\rho]}{\delta \rho} \right|_{\rho=\rho_A}$ cannot be reconstructed. The non-decomposable strategy is motivated by the fact that there are exact properties of $v_t[\rho_A, \rho_B](\vec{r})$, which can be taken into account quite easily in $\tilde{v}_t[\rho_A, \rho_B](\vec{r})$, whereas building-in them into some approximate functional $\tilde{T}_s[\rho]$ is less straightforward. Abandoning the decomposable strategy is motivated also by the results of our recent dedicated studies of the accuracy of various gradient-dependent approximations to $T_s^{nad}[\rho_A, \rho_B]$, which revealed that there is no correlation between the accuracy of $\tilde{T}_s^{nad}[\rho_A, \rho_B]$, $\tilde{v}_t[\rho_A, \rho_B](\vec{r})$ and the errors in the parent gradient-dependent approximation to $\tilde{T}_s[\rho]$ [33]. It should be also pointed out that, that the individual contributions $\tilde{T}_s^{nad}[\rho_A, \rho_B]$ are not needed in practice.

The non-decomposable approximation to $v_t[\rho_A, \rho_B](\vec{r})$ is constructed by enforcing the following exact conditions into its analytic form:

- $\tilde{T}_s^{nad}[\rho_A, \rho_B] \longrightarrow \tilde{T}_s^{nad(LDA)}[\rho_A, \rho_B]$ for uniform ρ_A and ρ_B .
- $\tilde{T}_s^{nad}[\rho_A, \rho_B] \longrightarrow 0$ for non-overlapping ρ_A and ρ_B .
- $\tilde{v}_t[\rho_A, \rho_B] \longrightarrow v_t^{limit}[\rho_B]$ at $\rho_A \longrightarrow 0$ and $\int \rho_B d\vec{r} = 2$.

The first two conditions are automatically satisfied by the decomposable gradient-expansion based approximations discussed in the previous section. Since such approximations proved to be sufficiently accurate for many systems the same conditions are retained in the new construction. The last condition is the key element of the present construction.

Before proceeding to the construction of the approximation obeying the considered exact condition we note that $v_t[\rho_A, \rho_B](\vec{r})$ can be alternatively

expressed as:

$$v_t[\rho_A, \rho_B] = \tilde{v}_t^{decomposable}[\rho_A, \rho_B] + f[\rho_A, \rho_B] \cdot v_t^{limit}[\rho_B] \quad (15)$$

All functionals in the above equation are determined locally and the argument \vec{r} is not written explicitly for simplicity and the functionals $v_t[\rho_A, \rho_B]$ and $f[\rho_A, \rho_B]$ are simply related ($f[\rho_A, \rho_B] = \frac{v_t[\rho_A, \rho_B] - \tilde{v}_t^{decomposable}[\rho_A, \rho_B]}{v_t^{limit}[\rho_A, \rho_B]}$ if $v_t^{limit}[\rho_A, \rho_B]$ is non-zero). The above form of $v_t[\rho_A, \rho_B]$ provides a convenient for construction of approximation. It can be used for any decomposable approximation to $v_t[\rho_A, \rho_B]$, which violates the considered condition, and the functional $f[\rho_A, \rho_B]$ has a clear physical meaning as a *switching factor* determining whether it is needed to add locally the missing component of the embedding potential. As far as the choice for the decomposable component, both the gradient-free potential given in Eq. 11 and the decomposable potential derived from the Lembarki-Chermette [36] approximation to $T_s[\rho]$ were shown in dedicated studies [32, 33] to be reasonably accurate if ρ_A and ρ_B do not overlap strongly. Both these approximations comprise the zeroth order contribution. If $\tilde{v}_t^{TF}[\rho_A, \rho_B]$ is used as decomposable component in Eq. 15, the terms $v_t^{limit}[\rho_B]$ and $\tilde{v}_t^{decomposable}[\rho_A, \rho_B]$ are local functions depending explicitly on ρ_A , ρ_B , $\nabla\rho_B$, and $\nabla^2\rho_B$. Approximating $f[\rho_A, \rho_B]$ by a local function depending explicitly on these quantities applied in Eq. 15 leads to an approximated potential requiring a similar computational effort as conventional low-order gradient-expansion based decomposable approximations to $v_t[\rho_A, \rho_B]$. The first approximation made here is replacing the switching factor defined in Eq. 15 by a *switching function*:

$$f[\rho_A, \rho_B](\vec{r}) \approx \tilde{f}(\rho_A, \rho_B, \nabla\rho_B, \nabla^2\rho_B) \quad (16)$$

The above considerations lead to the following general form of the approximation to $v_t[\rho_A, \rho_B](\vec{r})$:

$$\tilde{v}_t[\rho_A, \rho_B] = \tilde{v}_t^{TF}[\rho_A, \rho_B] + \tilde{f}(\rho_A, \rho_B, \nabla\rho_B, \nabla^2\rho_B) \cdot v_t^{limit}[\rho_B] \quad (17)$$

The above general form provides a clear interpretation for the switching function, which can be used as guideline in construction of approximations - it “detects” such volume elements for which the conditions $\rho_A \rightarrow 0$ and $\int \rho_B d\vec{r} = 2$ are most relevant.

3.1 The switching function \tilde{f} for environments comprising one-nucleus and two-electrons

In constructing $\tilde{f}(\rho_A, \rho_B, \nabla\rho_B, \nabla^2\rho_B)$ the following additional requirements (simplifications) are made:

- $\tilde{f}(\rho_A, \rho_B, \nabla\rho_B, \nabla^2\rho_B)$ is one in the vicinity of a nucleus to account fully for the missing $\frac{\zeta}{r}$ component.
- The criterion for determining the range at which $v_t^{limit}[\rho_B]$ is nuclear number independent.
- $\tilde{f}(\rho_A, \rho_B, \nabla\rho_B, \nabla^2\rho_B)$ does not depend on ρ_A (to obtain the analytic form of $\tilde{T}_s^{nad}[\rho_A, \rho_B]$: ($f[\rho_A, \rho_B] \approx \tilde{f}[\rho_B]$))

The above criteria are very restrictive and leave us with not many choices. The last one leads to the following form of the switching factor:

$$f[\rho_A, \rho_B] \approx \tilde{f}(\rho_B, \nabla\rho_B, \nabla^2\rho_B) \quad (18)$$

Approximating $f[\rho_A, \rho_B]$ by some function $f(\rho_B)$ is one of possible further simplifications. It is, however, very unlikely that a ρ_B -based switching function could be universal. The electron density near the nucleus depends on the effective nuclear charge ζ [40] and varies strongly from atom to atom. It is possible, however, to design an ζ -independent criterion. To this end, we consider the reduced density gradient ($s_B(\vec{r})$) defined as:

$$s_B = \frac{|\nabla\rho_B|}{2(3\pi^2)^{1/3}\rho_B^{4/3}} \quad (19)$$

For ρ_B obtained from hydrogenic orbital $1s$ defined by some effective nuclear charge ζ , the following ζ -independent observations can be made: *i*) For $\rho_B^{1s} = 2|1s|^2$, $s_{r=0} = (6\pi)^{-1/3} = 0.376$, and *ii*) $v_t^{limit}[\rho_B^{1s}]$ changes sign from positive to negative at $s_{r=2/\zeta} = \exp(4/3) \cdot s_{r=0} = 1.426$. These observations suggest that the switching function can take a very simple and ζ -independent form

$$\tilde{f}(\rho_B, \nabla\rho_B) = \tilde{f}(s_B) = \Theta(s_B - s_B^{min}) \times \Theta(s_B^{max} - s_B) \quad (20)$$

where $\Theta(x) = 1$ for $x \geq 0$ and $\Theta(x) = 0$ for $x < 0$ and $s_B^{min} = 0.376$ and $s_B^{max} = 1.426$.

Since Eq. 1 can be used also to obtain forces [25], it is preferable to use a smooth switching from 0 to 1 instead of Θ in the above definition. The simplest form of such a switching functional has the Fermi-Dirac statistics form:

$$\tilde{f} = \left(\exp(\lambda(-s_B + s_B^{min})) + 1 \right)^{-1} \times \left(1 - \left(\exp(\lambda(-s_B + s_B^{max})) + 1 \right)^{-1} \right) \quad (21)$$

where the parameter λ determines the smoothness of the switch.

$\lambda = 500$ in Eq. 21 leads to equivalent results to that obtained with the step function $\Theta(x)$ (differences in dipole in the range of 10^{-6} Debye and orbital energies in the range of 10^{-10} hartree). All results discussed in this work are obtained with $\lambda = 500$. Smaller values corresponding to even “softer” switching can be also used in our numerical implementation but is not considered here in order to minimise the use of adjustable parameters.

A switching factor \tilde{f} constructed following the above restrictions can be used to investigate the importance of enforcing the exact limit for $v_t[\rho_A, \rho_B](\vec{r})$ at $\rho_A \rightarrow 0$ and $\int \rho_B d\vec{r} = 2$ but only in cases where the environment comprises one nucleus and two electrons. Not only the condition $\int \rho_B d\vec{r} = 2$ apply rigorously but the considerations leading to the ζ -independent values of s_B^{max} and s_B^{min} apply as well. Such model systems as $\text{Li}^+\text{-H}_2\text{O}$ and $\text{Be}^{2+}\text{-H}_2\text{O}$ complexes if the water molecule is considered as subsystem A and the cation as subsystem B (environment) fall into this category. At equilibrium geometry addition of $\tilde{f} \cdot v_t^{limit}[\rho_B]$ results in a desired effect on calculated properties for these complexes. The lowest unoccupied embedded orbital associated with subsystem A is indeed localised on the cation and its energy is shifted by 0.262 eV in the case of Li^+ and by 0.830 eV in the case of Be^{2+} . Addition of $\tilde{f} \cdot v_t^{limit}[\rho_B]$ reduces also the dipole moment of a water molecule in the vicinity of the cation by 0.071 Debye and 0.409 Debye for Li^+ and Be^{2+} , respectively. Such noticeable numerical effects obtained for systems, for which the condition $\int \rho_B d\vec{r} = 2$ applies rigorously, indicate clearly that the exact limit considered might be relevant for practical calculations where the environment is larger.

3.2 Fine-tuning of the thresholds in the switching function \tilde{f}

Using only universal parameters s_B^{min} and s_B^{max} is very appealing but the reasoning leading to their numerical values does not apply in real systems. It allows one to study the importance of the considered exact conditions but only in particular cases. The approximation to $v_t[\rho_A, \rho_B](\vec{r})$ defined in Eq. 17 and using the switching function given in Eq. 21 has, therefore, little practical value. The construction of the switching function described in the previous section and choice of the thresholds s_B^{min} and s_B^{max} in particular can be expected not to be adequate for other systems for the following reasons:

- The criterion $0.376 \leq s_B \leq 1.426$ applies at hydrogen nucleus where addition of $v_t^{limit}[\rho_B]$ is not expected to be needed. We recall here that it is the danger of a collapse of electron density on a doubly occupied hydrogenic $1s$ orbital provides the physical motivation for introducing the $v_t^{limit}[\rho_B]$. Moreover, numerical studies on molecular electron densities indicate clearly that enforcing the local behaviour of the density of the kinetic energy near nucleus corresponding to the von Weizsäcker expression leads indeed to significant improvements of the approximation to $T_s[\rho]$ for all nuclei except that of hydrogen [47].
- For heavier atoms, electron density at the nucleus comprises contributions from other orbitals than the hydrogenic $1s$. This can lead to the possibility that $v_t^{limit}[\rho_B]$ is negative although $s_B \leq 1.426$.
- The criterion $0.376 \leq s_B \leq 1.426$ might also be satisfied near stationary points of the electron density such as bond midpoints. It is very unlikely that the condition $\int \rho_B d\vec{r} = 2$ can be relevant to any volume element centred on a stationary points. Therefore addition of $v_t^{limit}[\rho_B]$ lacks formal justification there. Although the condition $0.376 \leq s_B$ assures that $v_t^{limit}[\rho_B]$ is not added at the stationary point, where $|\nabla\rho_B| = 0$, or in the close proximity to it, the numerical value of this threshold requires verification in real systems. It should be added at this point also that, if linear combination of atomic orbitals is used to construct embedded orbitals, the quality of description of the density at the nuclear cusp depends on the used basis set. A weaker criterion should be used in practice to assure that the $v_t^{limit}[\rho_B]$ is indeed added in the vicinity of the nucleus.

We start with the choice made for s_B^{max} . Numerical analyses in the systems discussed in the next section show that $v_t^{limit}[\rho_B]$ is negative locally even if s_B is smaller than 1.426 for heavier nuclei. This suggests that this threshold should be reduced. The smaller is the value for this threshold the less probably is inclusion of negative $v_t^{limit}[\rho_B]$, which is desired from the point of view of universality of this threshold, but it comes at the expense of losing a part of the desired effect at two-electron nuclei by reducing the range at which addition of $v_t^{limit}[\rho_B]$ applies. We use the model system considered in Appendix B to estimate the effect associated with the reduction of this range. The underlying assumption leading to the value of 1.426 is rigorously true in the model system. The desired effect of reducing the charge distribution on top of the nucleus is achieved mainly by adding $v_t^{limit}[\rho_B](\vec{r})$ very close to the nucleus i.e. where $s_B < 0.6$. Increasing further the value of the s_B threshold leads to smaller effect. Moreover, adding locally $v_t^{limit}[\rho_B]$ to the potential near the nucleus leads to negligible effect on orbital energies in the system considered in Appendix B (it reaches a peak of about 10^{-4} eV at $s_B = 1.426$). These results for the model system indicate that any choice for $0.6 < s_B^{max} < 1.426$ is acceptable. In real systems discussed in the next section, lowering the threshold from 1.426 to 0.9 assures that $v_t^{limit}[\rho_B]$ is added only if it is positive.

The fine-tuning of s_B^{min} follows other considerations. We note that, in the model system considered in Appendix B, s_B^{min} can be reduced even to zero without affecting the results because lower values of s_B than 0.376 do not occur near the nucleus. To make sure that no nuclei is overlooked even if the chosen atomic basis set in practical calculations is such that the exact relation $s_B = 0.376$ for $r \rightarrow 0$ cannot be rigorously satisfied, s_B^{min} is reduced from 0.376 to 0.3. This change leads to negligible numerical effects if ρ_B corresponds to atomic electron densities. For molecular ρ_B , retaining the criterion based on the s_B^{min} is necessary to avoid unjustified additions of $v_t^{limit}[\rho_B]$ near stationary points.

The criteria based only on s_B^{min} and s_B^{max} are not sufficient if the environment comprises hydrogen atoms because they are satisfied also at hydrogen nucleus. To avoid adding the $v_t^{limit}[\rho_B]$ near hydrogens, the proposed switching function includes additionally the criterion based on smallness of ρ_B . It is required that ρ_B is larger than the square of the $1s$ wave function of the hydrogen atom ($Z=1$) at $r = 0$ which equals to $1/\pi = 0.318$. Concerning ρ_B^{min} , increasing the idealised value of 0.318 to even 1 does not affect the results for hydrogen-free systems because the density on top of any nucleus,

which is heavier than hydrogen, is at least one order of magnitude larger. Increasing the value ρ_B^{min} is desired for the same reasons as the ones motivating the decrease of s_B^{min} . The value of $\rho_B^{min} = 0.7$ was arbitrary chosen for practical calculations.

The final form of the “fine-tuned” switching function of more general applicability and used in the subsequent section for studying the importance of imposing the considered exact limit in real systems take the following form:

$$\begin{aligned} \tilde{f} &= \left(\exp(\lambda(-s_B + s_B^{min})) + 1 \right)^{-1} \times \left(1 - \left(\exp(\lambda(-s_B + s_B^{max})) + 1 \right)^{-1} \right) \\ &\times \left(\exp(\lambda(-\rho_B + \rho_B^{min})) + 1 \right)^{-1} \end{aligned} \quad (22)$$

where $s_B^{min} = 0.3$, $s_B^{max} = 0.9$, $\rho_B^{min} = 0.7$.

Eqs. 11, 14, 17, and 22 define the potential which will be referred to as $\tilde{v}_t^{NDSD}[\rho_A, \rho_B]$, (Non-Decomposable approximation using first- and Second Derivatives of ρ). The notion of non-decomposability is brought up here because the the second term in Eq. 17 does not have the form of a difference between two functional derivatives of some common explicit density functional $\tilde{T}_s[\rho]$. The analytic expression for $\tilde{T}_s^{nad(NDSD)}[\rho_A, \rho_B]$, which yields $\tilde{v}_t^{NDSD}[\rho_A, \rho_B]$ after functional differentiation with respect to ρ_A can be easily constructed. Its decomposable component is given in Eq. 10 and the non-decomposable $v_t^{limit}[\rho_B]$ component is ρ_A independent. The functional generating $v_t^{NDSD}[\rho_A, \rho_B]$ reads therefore:

$$\begin{aligned} \tilde{T}_s^{nad(NDSD)}[\rho_A, \rho_B] &= C_{TF} \int \left((\rho_A + \rho_B)^{5/3} - \rho_A^{5/3} - \rho_B^{5/3} \right) d\vec{r} \\ &+ \int f(\rho_B, \nabla \rho_B) \cdot \rho_A(\vec{r}) \tilde{v}_t^{limit}[\rho_B](\vec{r}) d\vec{r} + C[\rho_B] \end{aligned} \quad (23)$$

where $C[\rho_B]$ is ρ_A -independent. To assure the proper dissociation limit $C[\rho_B]$ must vanish.

4 Numerical validations

Procedure to analyse \tilde{v}_t -generated errors

In practical applications of Eq. 1, the results depend on ρ_B as well as on the used approximation to $v_t[\rho_A, \rho_B](\vec{r})$. As far as the quality of the used approximation to $v_t[\rho_A, \rho_B](\vec{r})$ is concerned, a general procedure was proposed in one

of our earlier works [33, 34]. Its principal element is the comparison between numerical values of the calculated property (energy components, dipole moments, total electron density, etc.) obtained from two fully variational formal frameworks: that of Cortona [21] and that of Kohn and Sham [7]. Results obtained from both frameworks are not exact but the difference between them can be attributed only to the approximation used for $v_t[\rho_A, \rho_B](\vec{r})$ if all technical parameters (approximation to the exchange-correlation functional, basis sets for expanding orbitals, algorithms to calculate used matrix elements) are the same. We point out here, however, that direct comparisons between the total electron densities derived from Kohn-Sham- and Cortona's calculations are cumbersome because these quantities are local. In practice, it is more convenient to use global quantities (norm of the difference between these densities, or selected observables) in such analyses (see the next section).

To obtain the pair of electron densities ρ_A and ρ_B which minimises the total energy in Cortona's type of calculations, a self-consistent super cycle of embedding calculations (*freeze-and-thaw* cycle) is performed. At each iteration, Eq. 1 are solved. In the subsequent iteration, ρ_A and ρ_B exchange their role in Eqs. 1. The *freeze-and-thaw* iterations continue until self-consistency. In the end, a pair of electron densities (ρ_A^0 and ρ_B^0) and the corresponding two sets of embedded orbitals is obtained. Obviously, the notion of *embedded system* and its *environment* becomes meaningless because both subsystems are treated on the equal footing. *Freeze-and-thaw* calculations are conducted in practice for small model systems to validate the used ρ_B in large scale multi-level numerical simulations [16] or, as it is made in the present work, to assess the used approximation to $v_t[\rho_A, \rho_B](\vec{r})$.

The \tilde{v}_t -generated errors in the complexation induced dipole moments due to violation of the limit for v_t at $\rho_A \rightarrow 0$ and $\int \rho_B d\vec{r} = 2$.

\tilde{v}_t -generated errors in complexation induced dipole moments can be expected to be strongly affected by the local behaviour of the used $\tilde{v}_t[\rho_A, \rho_B](\vec{r})$ near nuclei. Lack of sufficient repulsion near the nucleus might lead to an artificial transfer of electron density between subsystems reflected in the numerical values of the dipole moment. Therefore, this quantity was chosen for the analysis of the \tilde{v}_t -generated errors in a representative set of intermolecular

complexes including charged, polar and non-polar ones at their equilibrium geometries. For key details of the numerical implementation of the relevant equations, see Ref. [49].

Tables 1 and 2 collect the complexation induced dipole moments in neutral or charged complexes, respectively. First of all, switching on the $v_s^{limit}[\rho_B](\vec{r})$ term decreases the \tilde{v}_t -generated errors in each of the considered cases. For systems comprising neutral subsystems the effect on the errors are negligible. This indicated that the origin of the errors lies not in the violation the condition considered in this work. For systems comprising charged components, the effect of imposing the considered limit is evident. The errors are invariably reduced. The reduction of the relative errors depends on the system from such a case as $\text{Li}^+\text{-H}_2\text{O}$ (from 9.8% to 7.9%) to a reduction by factor 2 or 3 in $\text{Na}^+\text{-Br}^-$ and (from 1.4% to 0.7%) and $\text{Na}^+\text{-H}_2\text{O}$ (from 0.23% to 0.07%). Similarly as in the group of complexes formed by neutral molecules, the origin for the remaining errors lies somewhere else. The above numerical examples lead to the following principal conclusions:

- Violation of the limit for $v_t[\rho_A, \rho_B](\vec{r})$ at $\rho_A \rightarrow 0$ and $\int \rho_B d\vec{r} = 2$ contributes to the overall error in the calculated quantities but this contribution varies from one system to another. It is rather negligible for complexes formed by neutral components. It is numerically significant for complexes comprising charged components.
- Our simple strategy to impose the considered limit locally in the vicinity of nuclear cusps leads invariably to reduction of errors. Therefore it can be used generally as correction to any approximation violating the above limit.
- The construction of the approximation obeying the considered limit, and the used switching criteria in particular, corresponds to a real case where a distant nucleus is surrounded by a frozen-density shell comprising two electrons (He, Li^+ , Be^{2+} , etc.). The fact that the errors are reduced also for systems, where these idealised conditions do not apply, indicates that the considered condition is important and should be taken into account in construction of approximations to $v_t[\rho_A, \rho_B](\vec{r})$.
- For systems, where \tilde{v}_t -generated errors were not reduced by imposing the considered exact limit, their origin must be looked for somewhere else.

The effect of imposing the limit for v_t at $\rho_A \rightarrow 0$ and $\int \rho_B d\vec{r} = 2$ on orbital energies

In this section, we analyse the complexation induced shifts of orbital energies derived using the approximated potential $\tilde{v}_t^{NDS D}[\rho_A, \rho_B](\vec{r})$ considered in the previous section. Opposite to the dipole moments discussed previously, direct comparisons between the calculated shifts and the corresponding reference data are less straightforward. However, we investigate the numerical effect associated with imposing the exact limit for $v_t[\rho_A, \rho_B](\vec{r})$ at $\rho_A \rightarrow 0$ and $\int \rho_B d\vec{r} = 2$ in view of the numerical practice which indicates that shifting the levels of unoccupied orbitals localised in the environment would be desirable. Conventional decomposable approximations to $v_t[\rho_A, \rho_B](\vec{r})$ lead to artificially low levels of unoccupied orbitals in the environment which might cause unphysical effects such as charge-transfer between subsystems [43] or erroneous other observables [42].

The numerical results for a model system considered in Appendix B show that inclusion of the $v_t^{limit}[\rho_B]$ term everywhere where $0.6 \leq s_B \leq 0.9$ into the effective embedding potential leads to a positive shift of the energy level of the unoccupied orbital. In real intermolecular systems, the conditions considered in Appendix B ($\rho_A \rightarrow 0$ and $\rho_B = 2|1s|^2$) are not satisfied. The subsystems are in finite separation and the use of atom-centred basis sets for each subsystem, which include all atoms (supermolecular expansion labelled as KSCED(s) in Ref. [45]), results in the fact that ρ_A can be significant at a nucleus associated with subsystem B . For the same reasons and the fact that the considered nuclei include also atoms with occupied $2s$ shell, also the second assumption is not satisfied rigorously. Therefore, it is useful to verify in practice to which extent inclusion of the $v_t^{limit}[\rho_B]$ term affects the orbital levels if these asymptotic conditions do not apply.

Tables 3 and 4 collect the values of energy levels corresponding to the lowest lying orbital localised mainly in the environment for the previously considered complexes. The calculations are made not in the end of the *freeze-and-thaw* cycle but for the same ρ_B obtained from Kohn-Sham calculations for the isolated subsystem B. Including $v_t^{limit}[\rho_B]$ leads to the shifts of the energy levels of unoccupied orbitals of the magnitude which is significantly larger than that in the model system. It is a very desired effect of the new approximation.

In the $\text{Li}^+\text{-H}_2\text{O}$ case discussed in Ref. [42], the energy of the lowest unoccupied embedded orbital localised on Li^+ crosses that of the highest occupied

embedded orbital localised on H₂O at the intermolecular distance of 13 Å if Eq. 11 is used for $v_t[\rho_A, \rho_B](\vec{r})$. At larger separations, the self-consistent procedure to solve Eqs. 1 does not converge due to localisation of the highest occupied embedded orbital which jumps between subsystems in subsequent iterations. Addition of the $v_t^{limit}[\rho_B]$ term shifts the energy of the unoccupied embedded orbital localised at Li⁺. As the result, no crossing of levels occurs even at intermolecular separations as large as 18 Å. The occupied levels are affected less strongly (see Tables 5 and 6).

5 Discussion

In principle, any decomposable approximation can be used as the first term of Eq. 17 instead of the term derived from Thomas-Fermi functional. In the approximation introduced in this work, the decomposable component of $\tilde{v}_t^{NDSD}[\rho_A, \rho_B]$ is gradient-free and does not contribute to the asymptotic local behaviour of $v_t[\rho_A, \rho_B](\vec{r})$ at the nuclei. Only the second term enforces the desired behaviour. Should a gradient-dependent alternative for the first term be considered, a proper care should be taken to avoid double-counting of $v_t^{limit}[\rho_B]$ at a nucleus. For instance, $\tilde{v}_t^{GEA2}[\rho_A, \rho_B]$ comprises already 1/9 of $v_t^{limit}[\rho_B]$. To verify whether further improvements are possible following this lines, two approximations were considered by replacing $\tilde{v}_t^{TF}[\rho_A, \rho_B]$ in Eq. 17 by either $\tilde{v}_t^{GEA2}[\rho_A, \rho_B]$ [9] or $\tilde{v}_t^{GGA97}[\rho_A, \rho_B]$ [32]. Including the $v_t^{limit}[\rho_B]$ term into $\tilde{v}_s[\rho_A, \rho_B](\vec{r})$ brings improvements in both cases (see Table 7). This indicates $v_t^{limit}[\rho_B]$ should be enforced universally on any approximation to $v_s[\rho_A, \rho_B](\vec{r})$. Compared to the results obtained using $\tilde{v}_s^{NDSD}[\rho_A, \rho_B](\vec{r})$ discussed earlier in this work, the two alternative non-decomposable approximations $v_s[\rho_A, \rho_B](\vec{r})$ are not better.

We recall here the main reasons for singling out $\tilde{v}_t^{GGA97}[\rho_A, \rho_B]$ among other decomposable ones which depend explicitly on densities ρ_A and ρ_B as well as their first- and second derivatives.

- $\tilde{v}_t^{GEA2}[\rho_A, \rho_B]$ obtained from the second-order gradient-expansion approximation leads typically to worse results than that obtained from zeroth order [33, 45] indicating that the contribution to $v_t[\rho_A, \rho_B]$ due to the second term in Eq. 12 is erroneous. The deterioration of the results is pronounced the most at very small overlaps between ρ_A and ρ_B . Note that in the present work this flaw of $\tilde{v}_t^{GEA2}[\rho_A, \rho_B]$ manifests

itself in the absence of convergent solutions of Eq. 1 in $\text{Na}^+\text{-Cl}^-$ and $\text{Li}^+\text{-H}_2\text{O}$ cases (see Table 7).

- $\tilde{v}_t^{GGA97}[\rho_A, \rho_B]$ was introduced as a pragmatic solution replacing $\tilde{v}_t^{GEA2}[\rho_A, \rho_B]$. Due to its analytic form, the gradient-dependent contribution disappears at small overlaps between ρ_A and ρ_B .
- The functional $\tilde{T}^{LC94}[\rho]$ generating the decomposable approximated potential $\tilde{v}_s^{GGA97}[\rho_A, \rho_B]$ is known to be a very good approximation to $T_s[\rho]$.

The above reasons for singling out $\tilde{v}_t^{GGA97}[\rho_A, \rho_B]$ are not applicable for the non-decomposable construction presented in this work. In $\tilde{v}_t^{NDSD}[\rho_A, \rho_B]$ the problematic second-order term lying at the origin of flaws of $\tilde{v}_t^{GEA2}[\rho_A, \rho_B]$ is either present where it is needed to assure the correct asymptotic limit (i.e. in the vicinity of nuclei) or absent. Numerical results collected in Tables 1, 2, and 7 support fully the above formal reasons to consider $\tilde{v}_t^{NDSD}[\rho_A, \rho_B]$ as the successor of $\tilde{v}_t^{GGA97}[\rho_A, \rho_B]$.

6 Conclusions

Enforcing the considered exact limit for $v_t[\rho_A, \rho_B](\vec{r})$, as it is made in the proposed approximation, leads to a significant reduction of \tilde{v}_t -generated errors for charged systems. Errors in the complexation indexed dipole moments are reduced by more than 50% in some cases. For neutral systems, reduction of error takes also place but its magnitude is typically negligible. This indicates that one of important sources of inaccuracies in the conventional (i.e. decomposable and gradient-expansion based) approximations to $v_t[\rho_A, \rho_B](\vec{r})$ was identified. The origin of the remaining contributions \tilde{v}_t -generated errors lies probably somewhere else. The analytic form of the component of the local embedding potential enforcing the correct considered limit is, indeed, an approximation to $v_t[\rho_A, \rho_B](\vec{r})$ because its position dependency is indirect - through the density and its gradient. The function which was used to switch on the exact limit was designed based on the analysis of model system of relevance for elements of the first-, second- and the third period. Using the local potential introduced in this work ($\tilde{v}_t^{NDSD}[\rho_A, \rho_B](\vec{r})$ given in Eq. 17) as an alternative to potentials derived using conventional strategy of deriving it from analytic form of functionals based on low-order terms in the gradient

expansion of $T_s[\rho]$ [30] is recommended for the following reasons:

i) Formal: We believe that a proper strategy to improve approximations to functionals in density functional theory should proceed by imposing the most relevant exact conditions and $\tilde{v}_t^{NDSD}[\rho_A, \rho_B](\vec{r})$ was constructed in this way.

ii) Practical: The numerical results reported in this work show indeed that imposing this condition improves the obtained electron density and that the improvement varies from negligible to significant depending on the system.

iii) Numerical: Evaluating $\tilde{v}_t^{NDSD}[\rho_A, \rho_B](\vec{r})$ involves the same quantities as evaluating its counterparts derived from gradient-expansion- (up to second order) and so called generalised gradient approximations to $T_s[\rho]$.

Concerning the area of applicability of $\tilde{v}_t^{NDSD}[\rho_A, \rho_B](\vec{r})$, it should be underlined that some arbitrary choices were made concerning the criteria for “detecting” the vicinity of a nucleus based only on electron density ρ_B and its derivatives in the construction of this approximation. The chosen criteria are most adequate for such nuclei, where the total electron density is dominated by the hydrogenic $1s$ orbital.

The local potential $\tilde{v}_t^{NDSD}[\rho_A, \rho_B](\vec{r})$ introduced in this work is intrinsically non-decomposable. Although the analytic form of the functional $\tilde{T}_s^{mad(NDSD)}[\rho_A, \rho_B]$ and the potential $\tilde{v}_t^{NDSD}[\rho_A, \rho_B](\vec{r})$ are given in this work, the analytic form of neither $\tilde{T}_s^{NDSD}[\rho]$ nor $\frac{\delta \tilde{T}_s^{NDSD}[\rho]}{\delta \rho}$ is available. Therefore, the introduced here non-decomposable strategy can be seen as the first attempt to decouple the search for $\tilde{T}_s[\rho]$ and its functional derivative, which are needed in orbital-free calculations, from the search for an adequate approximation for the kinetic-kinetic-energy dependent component of the effective orbital-free embedding potential. Opposite to orbital-free strategy [31], neither $\tilde{T}_s[\rho]$ nor its functional derivative are needed in methods applying orbital-free effective embedding potential given in Eq. 7.

Finally, imposing the exact limit for $v_t[\rho_A, \rho_B](\vec{r})$ at $\rho_A \rightarrow 0$ and $\int \rho_B d\vec{r} = 2$ leads to shifts of the level of the unoccupied orbitals localised in the environment. Such shift is strongly desired in view of the earlier reports on possible practical inconveniences resulted from artificially low position of such levels when approximations not taking into account the cusp condition are used [42, 43].

Acknowledgement: This work was supported by Swiss National Science Foundation.

References

- [1] E.G. McRae, *J. Phys. Chem.*, **61** (1957) 562.
- [2] O. Tapia and O. Goscinski, *Mol. Phys.*, **29** (1975) 1653.
- [3] J. Åquist and A. Warshel, *Chem. Rev.*, **93** (1993) 2523; J. Gao, in: *Reviews in computational chemistry* vol. 7 eds. K.B. Lipkowitz and D.B. Boyd (VCH Publishers, New York, 1996) 119; J. Sauer, P. Ugliengo, E. Garrone, V.R. Saunders, *Chem. Rev.*, **94** (1994) 2095.
- [4] J.C. Phillips, L. Kleinman, *Phys.Rev.*, **116** (1959) 287.
- [5] T.M. Henderson, *J. Chem. Phys.*, **125**, 2006, 014105.
- [6] P. Hohenberg, W. Kohn, *Phys. Rev. B*, **136** (1964) 864.
- [7] W. Kohn, L.J. Sham, *Phys. Rev.* **140** (1965) A1133.
- [8] M. Levy, *Proc. Natl. Acad. Sci. USA*, **76** (1979) 6062.
- [9] T.A. Wesolowski, A. Warshel, *J. Phys. Chem.*, **97** (1993) 8050.
- [10] T.A. Wesolowski, *One-electron Equations for Embedded Electron Density: Challenge for Theory and Practical Payoffs in Multi-Level Modeling of Complex Polyatomic Systems* In: *Computational Chemistry: Reviews of Current Trends - Vol. 10*, J. Leszczynski, Ed., World Scientific, 2006, pp. 1-82.
- [11] E.V. Stefanovitch, T.N. Truong, *J. Chem. Phys.*, **104** (1996) 2946.
- [12] W.N. Mei, L.L. Boyer, M.J. Mehl, M.M. Ossowski, H.T. Stokes, *Phys. Rev. B*, **61**, (2000) 11425.
- [13] J.R. Trail, D.M. Bird, *Phys. Rev. B*, **62**, (2000) 16402.
- [14] M. Zbiri, M. Atanasov, C. Daul, J.-M. Garcia Lastra, T.A. Wesolowski, *Chem. Phys. Lett.*, **397** (2004) 441-446.
- [15] F. Shimojo, R.K. Kalia, A. Nakano, P. Vashishta, *Computer Phys. Comm.*, **167** 151.

- [16] J. Neugebauer, C.R. Jacob, T.A. Wesolowski, E.J. Baerends *J. Phys. Chem. A*, **109** (2005) 7805.
- [17] M.H.M. Olsson, G.Y. Hong, A. Warshel, *J. Am. Chem. Soc.*, **125**, (2003) 5025.
- [18] N. Choly, G. Lu, E. Weinan, E. Kaxiras, *Phys. Rev. B*, **71** (2005) 094101.
- [19] C.R. Jacob, L. Visscher, *J. Chem. Phys.*, **125** (2006) 194104.
- [20] J. Neugebauer, E.J. Baerends, *J. Phys. Chem. A*, **110** (2006) 8786.
- [21] P. Cortona, *Phys. Rev. B*, **44** (1991) 8454.
- [22] T.A. Wesolowski, J. Weber, *Chem. Phys. Lett.*, **248** (1996) 71.
- [23] T.A. Wesolowski, F. Tran, *J. Chem. Phys.*, **118** (2003) 2072.
- [24] M. Iannuzzi, B. Kirchner, J. Hutter, *Chem. Phys. Lett.*, **421** (2006) 16.
- [25] M. Dulak, J. Kaminski, T.A. Wesolowski, *J. Chem. Theor. & Comput.*, (2007) **3** 735.
- [26] M.E. Casida, T.A. Wesolowski, *Intl. J. Quant. Chem.*, **96** (2004) 577.
- [27] T.A. Wesolowski, *J. Am. Chem. Soc.*, **126**, (2004) 11444.
- [28] T. Klüner, N. Govind, Y.A. Wang, E.A. Carter, *J. Chem. Phys.*, **116** (2002) 42.
- [29] T.A. Wesolowski, *Phys. Rev. A*, **77** 012504.
- [30] D.A. Kirzhnits, *Sov. Phys. JETP*, **5**, (1957) 64.
- [31] (a) L.H. Thomas, *Proc. Camb. Phil. Soc.*, **23** (1927) 542; (b) E. Fermi, *Z. Physik*, **48** (1928) 73.
- [32] T.A. Wesolowski, *J. Chem. Phys.*, **106** (1997) 8516.
- [33] Y.A. Bernard, M. Dulak, J.W. Kaminski, T.A. Wesolowski, *J. Phys. A.*, **41** (2008) 055302.
- [34] T.A. Wesolowski, H. Chermette, J. Weber, *J. Chem. Phys.*, **105** (1996) 9182.

- [35] H. Lee, C. Lee, R. G. Parr, *Phys. Rev. A.*, **44** (1991) 768.
- [36] A. Lembarki, H. Chermette, *Phys. Rev. A*, **50** (1994) 5328
- [37] P. Fuentealba, O. Reyes, *Chem. Phys. Lett.*, **232** (1995) 31.
- [38] F. Tran, T.A. Wesolowski, *Int. J. Quantum Chem.*, **89** (2002) 441.
- [39] A. Zupan, J.P. Perdew, K. Burke, M. Causa, *Int. J. Quantum Chem.*, **61** (1997) 835.
- [40] E. Clementi, D.L. Raimondi, *J. Chem. Phys.*, **38** (1963) 2686.
- [41] M. Dulak, T.A. Wesolowski, *J. Chem. Phys.*, **124** (2006) 16410.
- [42] C.R. Jacob, S.M. Beyhan, L. Visscher, *J. Chem. Phys.*, **126** (2007) 234116.
- [43] M. Dulak and T.A. Wesolowski, *unpublished results*
- [44] C.F. von Weizsaecker, *Z. Physik*, **96** (1935) 431.
- [45] T.A. Wesolowski, J. Weber, *Int. J. Quantum Chem.*, **61** (1997) 303.
- [46] Y. Tal, R. F. W. Bader, *Int. J. Quantum Chem.: Quantum Chem. Symp.* **12** (1978) 153.
- [47] F. Tran, T.A. Wesolowski, *Chem. Phys. Lett.*, **360** (2002) 209.
- [48] P.A.M. Dirac, *Proc. Cambridge Philos. Soc.*, **26** (1930) 376.
- [49] *i)* LDA approximation for exchange-correlation functional: exchange [48] and Vosko et al. parametrisation [51] of the Ceperley-Alder data [50], *ii)* TZP atomic basis sets of the STO type [52], *iii)* supermolecular expansion of electron density of each subsystem (KSCED(s) label in Ref. [45], *iv)* equilibrium geometries obtained from Kohn-Sham LDA calculations with TZP basis sets (available from the authors upon request), *v)* Numerical implementation of the \tilde{v}_s^{NDS} in ADF code [52] version ADF2007 downloaded from svn repository on 2007-05-23.
- [50] D.M Ceperley, B.J. Alder, *Phys. Rev. Lett.*, **45** (1980) 566.
- [51] S.H. Vosko, L. Wilk, M. Nusair, *Can. J. Phys.*, **58** (1980) 1200.

- [52] G. te Velde, F.M. Bickelhaupt, E.J. Baerends, C. Fonseca Guerra, S.J.A. van Gisbergen, J.G. Snijders, T. Ziegler, *J. Comput. Chem.*, **22** (2001) 931.
- [53] B. Fornberg, *Siam. Rev.*, **40** (1998) 685.
- [54] V. Weber, C. Daul, R. Baltensperger, *Comp. Phys. Comm.*, *163* (2004) 133.
- [55] MATLAB 2006 <http://www.mathworks.com/>

Appendix A

Orbital-free embedding potential for $\rho_A \rightarrow 0$ and $\rho_B = 2|1s|^2$

For small $\delta\rho$ such that $\delta\rho \rightarrow 0$,

$$\begin{aligned}
 \delta T_s^{nad}[\rho_A, \rho_B] &= T_s^{nad}[\rho_A + \delta\rho, \rho_B] - T_s^{nad}[\rho_A, \rho_B] \\
 &= T_s[\rho_A + \delta\rho + \rho_B] - T_s[\rho_A + \rho_B] - T_s[\rho_A + \delta\rho] + T_s[\rho_A] \\
 &= \int \frac{\delta T_s[\rho]}{\delta\rho}(\vec{r}) \Big|_{\rho=\rho_A+\rho_B} \delta\rho(\vec{r}) d\vec{r} - \int \frac{\delta T_s[\rho]}{\delta\rho}(\vec{r}) \Big|_{\rho=\rho_A} \delta\rho(\vec{r}) d\vec{r} + O(\delta^2\rho)
 \end{aligned} \tag{24}$$

If also ρ_A is small i.e. $\rho_A \rightarrow 0$,

$$T_s^{nad}[\rho_A + \delta\rho, \rho_B] - T_s^{nad}[\rho_A, \rho_B] = \int \frac{\delta T_s[\rho]}{\delta\rho}(\vec{r}) \Big|_{\rho=\rho_B} \delta\rho(\vec{r}) d\vec{r} + O(\delta^2\rho) \tag{25}$$

Therefore,

$$\frac{\delta T_s^{nad}[\rho, \rho_B]}{\delta\rho}(\vec{r}) \Big|_{\rho \rightarrow 0} \approx \frac{\delta T_s[\rho]}{\delta\rho}(\vec{r}) \Big|_{\rho \rightarrow \rho_B} \tag{26}$$

The above result that the kinetic-energy component of v_{emb}^{KSCED} is just the functional derivative of the $T_s[\rho]$ calculated for $\rho = \rho_B$ makes it possible to express it analytically for any ρ_B which comprises just two electrons. For one-electron and two-electron- spin-compensated systems the exact expression reads [44]:

$$T_s[\rho] = T_s^W[\rho] = \int \frac{1}{8} \frac{|\nabla|\rho|^2}{\rho} d\vec{r} \text{ for } \int \rho d\vec{r} = 2 \tag{27}$$

Therefore,

$$\frac{\delta T_s^W[\rho]}{\delta\rho} \Big|_{\rho=\rho_B} = \frac{1}{8} \frac{|\nabla\rho_B|^2}{\rho_B^2} - \frac{1}{4} \frac{\nabla^2\rho_B}{\rho_B} \text{ if } \int \rho_B d\vec{r} = 2 \tag{28}$$

Using Eq. 28 in Eq. 26 leads to the asymptotic form of the kinetic energy component of v_{emb}^{KSCED} in the case where ρ_A and ρ_B do not overlap significantly and ρ_B is a two-electron spin-less electron density reads:

$$\left. \frac{\delta T_s^{nad}[\rho, \rho_B]}{\delta \rho} \right|_{\rho=\rho_A \rightarrow 0, \int \rho_B d\vec{r}=2} = \frac{1}{8} \frac{|\nabla \rho_B|^2}{\rho_B^2} - \frac{1}{4} \frac{\nabla^2 \rho_B}{\rho_B} \quad (29)$$

ρ_B representing a doubly occupied hydrogenic $1s$ function ($1s = \sqrt{\zeta^3/\pi} \cdot \exp(-\zeta r)$) reads:

$$\rho_B^{1s}(\vec{r}) = \rho_B^{1s}(r) = 2 \cdot \zeta^3/\pi \cdot \exp(-2\zeta r), \quad (30)$$

For ρ_B^{1s} , Eq. 29 leads to the following potential:

$$\left. \frac{\delta T_s^{nad}[\rho, \rho_B]}{\delta \rho}(\vec{r}) \right|_{\rho=\rho_A \rightarrow 0, \rho_B=\rho_B^{1s}} = \frac{\zeta}{r} - \frac{\zeta^2}{2} \quad (31)$$

The potential given in Eq. 31 is repulsive for $r < \frac{2}{\zeta}$. For hydrogenic densities ρ_B^{1s} , the reduced density gradient equals to a ζ -independent value of 1.426. Near the nuclear cusp, therefore, a pair of electrons on the $1s$ shell provides a local repulsive potential which compensates the Coulomb attraction due to the nuclear charge. Note that the effective nuclear charge ζ for the most tightly bound orbital ($1s$) in a multi-electron atom is smaller than the charge of the corresponding nucleus (Z) [40]. As a consequence, the compensation is perfect only for one-electron hydrogenic systems.

Appendix B

The effect of approximations to $v_t[\rho_A, \rho_B](r)$ on the energies of bound states localised in the environment far from subsystem A

We consider numerical solutions of the Schrödinger equation for one electron in the spherically symmetric potential which takes the general form given in Eqs. 6-7. The analysed potential corresponds to $v_{eff}^{KS}[\rho_A; \vec{r}] = 0$, $v_{ext}^B(\vec{r}) = -\frac{Z}{r}$, and $v_{emb}^{KSCEd}[\rho_A, \rho_B; \vec{r}]$ defined in Eq. 7 for $\rho_A \rightarrow 0$ and $\rho_B = \rho_B^{1s}$. Such a case represents a local potential around a nucleus with the charge Z localised in the environment far from the investigated subsystem A and ρ_B comprising entire contribution from doubly occupied $1s$ shell centred on this nucleus. Dirac's exchange energy expression [48] is used to derive the exchange-correlation component of $v_{emb}^{KSCEd}[\rho_A, \rho_B; \vec{r}]$. The solutions of one-electron Schrödinger equation for such potential is obtained by radial quadrature described in Refs. [53, 54] implemented numerically using MATLAB2006 environment [55]. Finite difference approximation and the matrix representation with 127 radial points is used. The above model system is used to investigate the effect of approximations to $v_t[\rho_A, \rho_B](r)$ on the lowest energy level.

Using such approximate potential $\tilde{v}_t[\rho_A, \rho_B](r)$, which is finite at nuclear cusp, might lead to appearance of artificially stabilised bound states due to improper balance between the nuclear attraction, classical electron-electron repulsion, which are both described exactly and improperly behaving $\tilde{v}_t[\rho_A, \rho_B](r)$. This imbalance does not cause qualitative problems in the $Z=2$ (helium atom) case. No bound states occur if $v_t[\rho_A, \rho_B](r)$ is approximated by:

$$\begin{aligned} \tilde{v}_t^{model0} &= \left. \frac{\delta T_s^{nad(TF)}[\rho, \rho_B]}{\delta \rho} \right|_{\rho=\rho_A \rightarrow 0} \\ &= \frac{5}{3} C_{TF} \rho_B^{2/3} \end{aligned} \quad (32)$$

derived from the uniform-electron gas expression for v_t given in Eq. 11.

For $Z = 3$ (i.e. Li^+), however, \tilde{v}_t^{model0} leads to a bound state of the energy -0.2096654 hartree. This value will be used as a reference for analysis of other approximations to $v_t[\rho_A, \rho_B](\vec{r})$.

The expression derived from the second-order gradient approximation to $\frac{\delta T_s^{nad}[\rho_A, \rho_B]}{\delta \rho_A}$ reads:

$$\begin{aligned} \tilde{v}_t^{model1} &= \left. \frac{\delta T_s^{nad(GEA2)}[\rho, \rho_B]}{\delta \rho} \right|_{\rho=\rho_A \rightarrow 0} \\ &= \frac{5}{3} C_{TF} \rho_B^{2/3} - \frac{1}{72} \frac{\nabla^2 \rho_B}{\rho_B} + \frac{1}{144} \frac{|\nabla \rho_B|^2}{\rho_B^2} \end{aligned} \quad (33)$$

leads to a further lowering of the energy to -0.611935 hartree.

In the following part, other potentials will be considered, for which a local non-decomposable contribution is added to that given in Eq. 32 near the nucleus.

$$\begin{aligned} \tilde{v}_t^{model2}(r) &= \frac{5}{3} C_{TF} \rho_B^{2/3} \\ &+ \begin{cases} \frac{1}{8} \frac{|\nabla \rho_B|^2}{\rho_B} - \frac{1}{4} \frac{\nabla^2 \rho_B}{\rho_B^2} = \frac{\zeta}{r} - \frac{\zeta^2}{2} & \text{for } r \leq r^T \\ 0 & \text{for } r > r^T \end{cases} \end{aligned} \quad (34)$$

Figure 2 shows that, compared to the decomposable result, the addition of a non-decomposable component destabilises the energy but only for such small values of r at which $s_B \leq 1.6$. The maximal destabilisation occurs at $s_B = 1.426$ in line with the change of sign of the added term. A similar picture emerges from the analysis of the electron density at $r = 0$. Comparisons of Figures 2 and 3 reveals that addition of the non-decomposable term to the effective potential affects the orbital energies and electron density in a different manner. Even very close to the nucleus this addition reduced electron density without affecting the orbital energy noticeably. From the point of view of choosing s_B^{max} determining the range of this additional potential it is worthwhile to notice that the limit $s = 1.426$ should not be exceeded. The energy level starts a rapid descend and the on-top density starts to rise again at larger values of s_B^T . As far as the lower limit for s_B is concerned, it should not be smaller than about 0.5 because points at which $s_B < 0.5$ influence significantly the charge density at the nucleus.

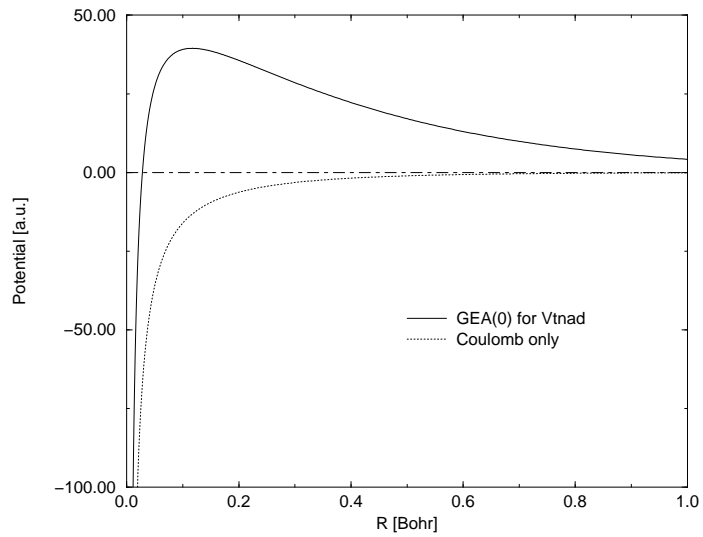


Figure 1: Effective potential (Eq. 7) calculated using local density approximation for its exchange- and kinetic energy components for: $\rho_B = \rho_{He}$, $\rho_A \rightarrow 0$, and $v_{ext}^B(\vec{r}) = -2/r$.

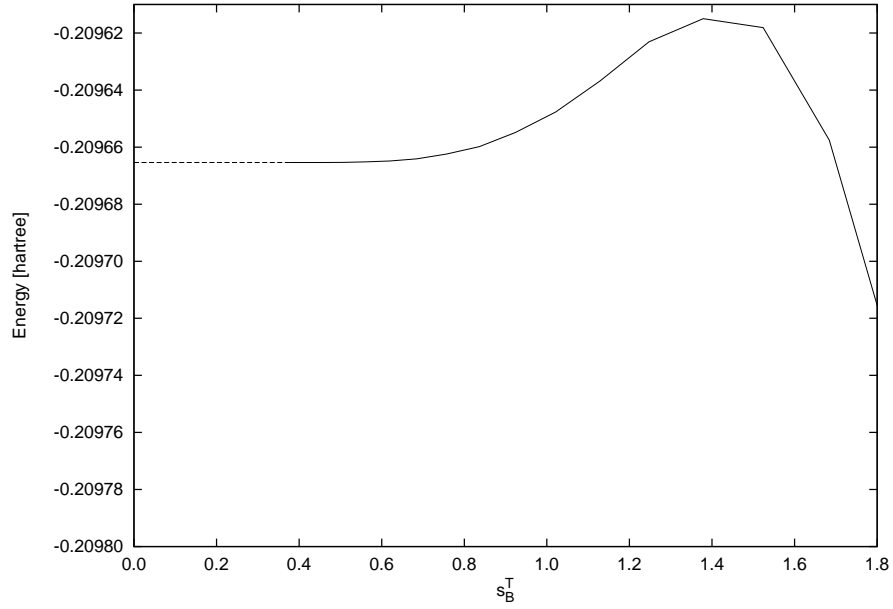


Figure 2: The ground-state energy level in the model system for different values of the threshold s_B^T corresponding to the range r^T of the $\frac{1}{8} \frac{|\nabla \rho_B|^2}{\rho_B} - \frac{1}{4} \frac{\nabla^2 \rho_B}{\rho_B^2}$ term in Eq. 34. For $s_B^T < 0.376$, the corresponding r^T does not exist in the model system and the results obtained without this additional term are shown.

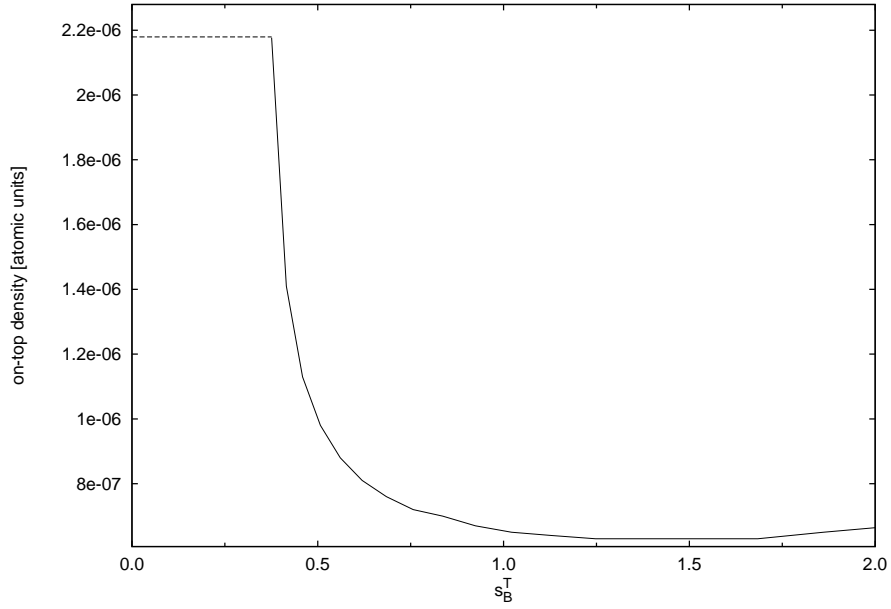


Figure 3: The electron density at $r = 0$ in the model system for different values of the threshold s_B^T corresponding to the range r^T of the $\frac{1}{8} \frac{|\nabla \rho_B|^2}{\rho_B} - \frac{1}{4} \frac{\nabla^2 \rho_B}{\rho_B^2}$ term in Eq. 34. For $s_B^T < 0.376$, the corresponding r^T does not exist in the model system and the results obtained without this additional term are shown.

Table 1: Total dipole moment (μ in Debye) obtained from the *freeze-and-thaw* calculations using two approximations $v_t[\rho_A, \rho_B](\vec{r})$. The target Kohn-Sham results are given for comparison. Only dipole moment components along the principal axis connecting the subsystems are given. Relative percentage errors of the dipole moments derived from subsystem based calculations ($\frac{\Delta\mu^{subsystem} - \Delta\mu^{Kohn-Sham}}{\Delta\mu^{Kohn-Sham}} 100\%$) are given in parentheses.

		freeze-and-thaw		Kohn-Sham
		Eq. 11	Eq. 17	
<i>A</i>	<i>B</i>	μ		
Li ⁺	F ⁻	5.429 (9.8)	5.542 (7.9)	6.020
Li ⁺	Cl ⁻	5.768 (15.5)	5.938 (13.0)	6.828
Li ⁺	Br ⁻	5.706 (18.9)	5.899 (16.1)	7.033
Na ⁺	F ⁻	7.576 (1.6)	7.612 (1.1)	7.697
Na ⁺	Cl ⁻	8.509 (1.2)	8.563 (0.5)	8.608
Na ⁺	Br ⁻	8.637 (1.4)	8.698 (0.7)	8.758
Be ²⁺	O ²⁻	4.225 (31.0)	4.363 (28.7)	6.120
Mg ²⁺	O ²⁻	6.741 (3.5)	6.822 (2.4)	6.988
H ₂ O	H ₂ O	2.669 (3.9)	2.670 (3.9)	2.779
HF	HF	3.000 (2.8)	3.000 (2.8)	3.090
He	CO ₂	0.014 (-8.6)	0.014 (-8.4)	0.013
Ne	CO ₂	0.027 (-7.6)	0.027 (-7.6)	0.025

Table 2: Total dipole moment (μ in Debye) obtained from the *freeze-and-thaw* calculations using two approximations $v_t[\rho_A, \rho_B](\vec{r})$. The target Kohn-Sham results are given for comparison. Only dipole moment components along the principal axis connecting the subsystems are given. Relative percentage errors of the dipole moments derived from subsystem based calculations ($\frac{\Delta\mu^{subsystem} - \Delta\mu^{Kohn-Sham}}{\Delta\mu^{Kohn-Sham}} 100\%$) are given in parentheses.

		freeze-and-thaw		Kohn-Sham
		Eq. 11	Eq. 17	
<i>A</i>	<i>B</i>	μ		
Li ⁺	H ₂ O	5.298 (3.91)	5.353 (2.91)	5.513
Li ⁺	F ₂	7.783 (0.31)	7.805 (0.03)	7.807
Li ⁺	CO ₂	9.387 (0.10)	9.403 (-0.07)	9.396
Na ⁺	H ₂ O	6.512 (0.23)	6.521 (0.07)	6.527
H ₃ O ⁺	Ar	2.681 (0.96)	2.683 (0.89)	2.707
NH ₄ ⁺	Ar	1.661 (8.52)	1.665 (8.33)	1.816
Be ²⁺	He	12.475 (3.94)	12.579 (3.14)	12.986
Be ²⁺	H ₂ O	12.066 (11.08)	12.336 (9.09)	13.569
Mg ²⁺	He	17.302 (0.20)	17.313 (0.14)	17.338
Mg ²⁺	H ₂ O	19.441 (1.57)	19.511 (1.22)	19.751

^a for charged systems the dipole moment is calculated for the cation at the origin.

Table 3: The effect of adding non-decomposable contribution to the embedding potential on the energy on the lowest unoccupied orbital localised in the environment (LUEO). For each complex, the used electron density of the environment (ρ_B) is the ground-state Kohn-Sham (LDA) electron density of the isolated subsystem B .

subsystem B	subsystem A	ϵ_{LUEO} $\tilde{v}_s = \tilde{v}^{TF}$	ϵ_{LUEO} $\tilde{v}_s = \tilde{v}^{NDSD}$	$\Delta\epsilon_{LUEO}$
Li ⁺	F ⁻	-2.249	-2.160	0.089
Li ⁺	Cl ⁻	-2.669	-2.568	0.101
Li ⁺	Br ⁻	-2.741	-2.635	0.106
Na ⁺	F ⁻	-1.908	-1.874	0.034
Na ⁺	Cl ⁻	-2.202	-2.164	0.038
Na ⁺	Br ⁻	-2.253	-2.214	0.039
Be ²⁺	O ²⁻	-4.922	-4.913	0.009
Mg ²⁺	O ²⁻	-4.634	-4.609	0.025

Table 4: The effect of adding non-decomposable contribution to the embedding potential on the energy on the lowest unoccupied orbital localised in the environment (LUEO). For each complex, the used electron density of the environment (ρ_B) is the ground-state Kohn-Sham (LDA) electron density of the isolated subsystem B .

subsystem B	subsystem A	ϵ_{LUEO} $\tilde{v}_s = \tilde{v}^{TF}$	ϵ_{LUEO} $\tilde{v}_s = \tilde{v}^{NDSD}$	$\Delta\epsilon_{LUEO}$
Li ⁺	H ₂ O	-7.533	-7.332	0.201
Li ⁺	F ₂	-8.501	-8.223	0.279
Li ⁺	CO ₂	-9.069	-8.810	0.259
Na ⁺	H ₂ O	-6.295	-6.240	0.055
Be ²⁺	He	-26.681	-25.797	0.884
Mg ²⁺	He	-18.376	-18.078	0.299
Be ²⁺	H ₂ O	-21.737	-21.172	0.565
Mg ²⁺	H ₂ O	-16.570	-16.327	0.242

Table 5: The effect of adding non-decomposable contribution to the embedding potential on the energy on the highest occupied embedded orbital (HOEO). For each complex, the used electron density of the environment (ρ_B) is the ground-state Kohn-Sham (LDA) electron density of the isolated subsystem B .

subsystem B	subsystem A	ϵ_{HOEO} $\tilde{v}_s = \tilde{v}^{TF}$	ϵ_{HOEO} $\tilde{v}_s = \tilde{v}^{NDSD}$	$\Delta\epsilon_{HOEO}$
Li ⁺	F ⁻	-6.716	-6.635	0.081
Li ⁺	Cl ⁻	-6.399	-6.339	0.060
Li ⁺	Br ⁻	-6.122	-6.068	0.054
Na ⁺	F ⁻	-5.223	-5.198	0.025
Na ⁺	Cl ⁻	-5.397	-5.379	0.018
Na ⁺	Br ⁻	-5.277	-5.261	0.016
Be ²⁺	O ²⁻	-6.724	-6.690	0.033
Mg ²⁺	O ²⁻	-5.135	-5.108	0.027
H ₂ O ^{<i>a</i>}	H ₂ O	-6.799	-6.799	0.000
HF ^{<i>a</i>}	HF	-9.450	-9.450	0.000
H ₂ O ^{<i>b</i>}	H ₂ O	-8.010	-8.011	-0.001
HF ^{<i>b</i>}	HF	-10.896	-10.896	0.000

^{*a*} acceptor of hydrogen bond

^{*b*} donor of hydrogen bond

Table 6: The effect of adding non-decomposable contribution to the embedding potential on the energy on the highest occupied embedded orbital (HOEO). For each complex, the used electron density of the environment (ρ_B) is the ground-state Kohn-Sham (LDA) electron density of the isolated subsystem B .

subsystem B	subsystem A	ϵ_{HOEO} $\tilde{v}_s = \tilde{v}^{TF}$	ϵ_{HOEO} $\tilde{v}_s = \tilde{v}^{NDS}$	$\Delta\epsilon_{HOEO}$
Li ⁺	H ₂ O	-14.530	-14.492	0.037
Li ⁺	F ₂	-16.507	-16.493	0.014
Li ⁺	CO ₂	-14.749	-14.742	0.007
Na ⁺	H ₂ O	-13.284	-13.278	0.006
Be ²⁺	He	-37.558	-37.306	0.252
Mg ²⁺	He	-31.410	-31.386	0.024
Be ²⁺	H ₂ O	-25.208	-25.001	0.207
Mg ²⁺	H ₂ O	-21.178	-21.131	0.047

Table 7: Total dipole moment (μ in Debye) obtained from the *freeze-and-thaw* calculations using different approximations $v_t[\rho_A, \rho_B](\vec{r})$. The target Kohn-Sham results are given in Tables 1 and 2. Only dipole moment components along the principal axis connecting the subsystems are given. Relative percentage errors of the dipole moments derived from subsystem based calculations ($\frac{\Delta\mu^{subsystem} - \Delta\mu^{Kohn-Sham}}{\Delta\mu^{Kohn-Sham}} 100\%$) are given in parentheses.

system	v_t^{GGA2}	$v_t^{GGA2} + f \cdot v_t^{limit}$	v_t^{GGA97}	$v_t^{GGA97} + f \cdot v_t^{limit}$
Li ⁺ Cl ⁻	5.365 (21.4)	5.519 (19.2)	5.671 (16.9)	5.829 (14.6)
Li ⁺ H ₂ O ^a	- ^b (-)	5.188 (5.9)	5.252 (4.7)	5.303 (3.8)
Na ⁺ Cl ⁻	- ^b (-)	8.025 (6.9)	8.346 (3.0)	8.400 (2.4)
Na ⁺ H ₂ O ^a	6.378 (2.3)	6.388 (2.1)	6.459 (1.0)	6.470 (0.9)
Be ²⁺ O ²⁻	3.962 (35.3)	4.073 (33.4)	4.128 (32.5)	4.245 (30.6)
HF HF	2.994 (3.1)	2.994 (3.1)	2.995 (3.1)	2.995 (3.1)

^a for charged systems the dipole moment is calculated for the cation at the origin. ^b no convergence.